Time-resolved rheology as a tool to monitor the progress of polymer degradation in the melt state – Part II: Thermal and thermo-oxidative degradation of polyamide 11/organo-clay nanocomposites

G. Filippone [a, *], S.C. Carroccio [b, **], G. Curcuruto [b], E. Passaglia [c], C. Gambarotti [d], N.Tz. Dintcheva [e]

[a] *Dipartimento di Ingegneria Chimica, dei Materiali e della Produzione Industriale (INSTM Consortium - UdR Naples), Università di Napoli Federico II, Piazzale V. Tecchio 80, 80125 Napoli, Italy*

[b] *Consiglio Nazionale delle Ricerche, CNR-IPCB UOS Catania, Via P. Gaifami 18, 95126 Catania, Italy*

[c] *Istituto di Chimica dei Composti Organometallici (ICCOM-CNR, UOS Pisa), Pisa, Italy*

[d] *Dipartimento di Chimica, Materiali e Ingegneria Chimica "Giulio Natta", Politecnico di Milano, Piazza L. da Vinci 32, 20133 Milano, Italy*

[e] *Dipartimento di Ingegneria Civile, Ambientale, Aerospaziale, dei Materiali, Università di Palermo, Viale delle Scienze, Ed. 6, 90128 Palermo, Italy*

Received 3 May 2015
Received in revised form
9 July 2015
Accepted 24 July 2015
Available online 26 July 2015

1. Introduction

Materials undergoing fast changes of their properties require specific experimental protocols able to elude the time evolution of the properties while testing. Polymer melts experiencing rapid degradation phenomena fall in this category of "transient materials", hence measuring their rheological properties can be challenging. In Part I we have shown how time-resolved mechanical spectroscopy (TRMS) can be profitably used for eluding changes in the rheological properties of polyamide 11 (PA11) due to degradation [1]. As a result of the high accuracy of data collected in this way, we have been able to relate the time evolution of rheological properties to the progress of thermal and thermo-oxidative degradation. Specifically, different reaction mechanisms have been conjectured solely based on the analysis of rheological data. The hypotheses have been corroborated through size exclusion chromatography and matrix-assisted laser desorption/ionization time-of-flight (MALDI-TOF) mass spectrometry. The issue that we are going to address now is assessing the potential of rheological analysis to study polymer degradation in systems more complex than neat polymers. In particular, we focus our attention on polymer nanocomposites (PNCs). This class of materials has attracted huge interest in the last decades, and is finding application in many

* Corresponding author.
** Corresponding author.
E-mail addresses: gfilippo@unina.it (G. Filippone), sabrinacarola.carroccio@cnr.it (S.C. Carroccio).

fields of modern technology [2]. Apart from this, the reason why we selected PNCs is that nanoparticles remarkably affect the flow behavior of the host matrix, possibly masking the polymer degradation phenomena to be studied via rheology. In particular, nanoparticles are well-known to move and rearrange in polymer melts, causing a gradual change over time of the rheological functions [3–5]. At the same time, alterations in the polymer rheology due to degradation in turn affect the nanoparticle dynamics; this adds further complications to the interpretation of rheological data. Additionally, nanoparticles can play an active role in the degradation pathways of the polymer matrix. This is the case of many organo-modified fillers, which are commonly used for producing PNCs due to their better dispersibility compared to bare nanoparticles. The organo-modifier can partially degrade during processing, and the degradation products can promote specific reactions involving the matrix [6]. To sum up, the overall rheological behavior of PNCs is the result of a complex interplay among various actors, who influence each other making particularly difficult the analysis of rheological data. Indeed, reological methods are seldom used to study PNC degradation, which is more commonly investigated by means of analytical techniques, such as IR/UV spectroscopy, chemiluminescence, size exclusion chromatography, gas chromatography, matrix-assisted laser desorption/ionization (MALDI) [7]. Here we test the potential of rheology for studying polymer degradation in PA11-based nanocomposites containing commercial organo-modified clay. This kind of nanoparticles is among the most used for producing PNCs because the starting clay materials are easily available, and their intercalation chemistry has been studied for a long time [8]. The rheology of PNCs based on organo-clays has been the subject of intensive research in the last decades. As far as we are concerned, the selected nanoparticles substantially alter the viscoelastic behavior at low frequencies [9,10], which is the regime in which polymer degradation is more plainly detectable. Another reason that led us to select organo-modified clay is its renowned interference with the degradation pathways of host polymers [11–14]. This makes the effect of nanoparticles on the rheology of PNCs not merely additional, and this is in line with our purpose of dealing with rheologically complex systems. The objective was pursued by means of a comparative analysis performed using neat PA11 as reference material. In more detail, profiting from the knowledge acquired in *Part I*, TRMS was used to monitor the viscoelasticity of PNCs during time. The hypotheses about the degradation mechanisms of PA11 in the presence of nanoparticles were corroborated through analytical techniques, namely oxidative induction time (OIT) measurements and MALDI-TOF mass spectrometry. The latter allowed to detect chain scission reactions deriving from hydrolysis and/or α-CH Hydrogen abstraction processes [15]. Finally, the effect of nanoparticle loading was studied to critically discuss the limits of rheology when the flow behavior is dominated by the filler.

2. Experimental

2.1. Raw materials and sample preparation

The PA11 (Sigma–Aldrich) has $\rho = 1.026$ g cm^{-3} at $T = 25$ °C, glass transition temperature $T_g = 46$ °C and melting temperature $T_m = 198$ °C. The filler is an organo-modified clay supplied by Southern Clay Products with trade name of Cloisite® 30B; it is a montmorillonite modified by 0.09 equiv. per 100 g of bis(2-hydroxylethyl)methyl tallow alkylammonium cations. 2-(4 hydroxyphenilazo)benzoic acid (HABA) and hexafluoroisopropanol (HFIP) were purchased from Aldrich Chemical CO (Italy) and used as supplied.

Nanocomposite samples at 3 and 9 wt.-% of organo-clay, hereinafter referred as PA11-C3 and PA11-C9, respectively, were prepared by using a co-rotating twin-screw extruder (DSM Xplore) equipped with a cylindrical capillary die (diameter 1.5 mm, length 30 mm). The polymer and the filler, both dried overnight under vacuum at $T = 80$ °C for 18 h, were simultaneously loaded inside the mixing apparatus. The extrusions were performed under gaseous nitrogen at $T = 215$ °C and screw speed 80 rpm, corresponding to average shear rates of ~50 s^{-1}. The residence times, carefully controlled owing to an integrated back-flow channel, were set to 2 min. Preliminary investigations indicated that such conditions represent a good compromise to get adequate filler dispersion while preserving the stability of polymer matrices and clay organo-modifier.

Rheological, TEM and calorimetric (OIT) analyses were performed on as-extruded pellets. The samples for MALDI investigations were prepared by dissolving in HFIP pellets treated under either N_2 or air atmosphere at $T = 215$ °C for 30, 60, 90, 120 and 150 min. The solutions were filtered and dried before the analyses. Insoluble fractions of dry solid, if any, were dried under vacuum and weighed. WAXD analyses were performed on compression-molded films prepared by means of a laboratory press (LP-20B by Lab. Tech. Eng. Company Ltd.).

2.2. Characterization

Wide angle X-ray diffractometry (WAXD) was performed using a Siemens D-500 diffractometer with Cu Kα radiation ($\lambda = 0.154$ nm). Scans were taken from $2\theta = 2$–10° with a step size of 0.02°.

Transmission electron microscopy (TEM) was performed using a Philips CM 200 TEM. The samples were thin slices (thickness ~100 nm) randomly cut from the extruded pellets using a diamond knife at room temperature.

Rheological analyses were carried out using a stress-controlled rotational rheometer (AR-G2 by TA Instruments) in parallel plate geometry (plate diameter 40 mm). The as-extruded pellets, dried for 18 h at $T = 80$ °C under vacuum, were compacted between the plates of the rheometer by means of a containment ring just before running the rheological tests. Repeated frequency scans were performed at $T = 215$ °C from frequency $\omega = 10^{-1}$ up to 10^2 rad s^{-1}, and the elastic (G') and viscous (G'') shear moduli were recorded as a function of time at strain amplitude low enough to be in the linear regime. The latter was preliminarily estimated for each sample through strain scan experiments. Measurements were carried out both in air and gaseous nitrogen atmosphere.

Thermogravimetric analysis (TGA) was carried out using a Seiko EXSTAR 7200 TGA/DTA instrument. Analyses were carried out on 5–10 mg samples under either nitrogen or air flow (200 ml/min) from room temperature up to 700 °C at a heating rate of 10 °C/min.

Oxidation induction time (OIT) measurements were performed using a differential scanning calorimeter DSC 400 (Perkin Elmer) according to the testing procedure of ISO 11357-6-2008. Samples of approximately 5 mg were heated up to 215 °C at a rate of 20 °C/min under nitrogen flow (50 ml/min) and kept at this temperature for 15 min to ensure complete melting and to attain thermal equilibrium. After, the gas was switched to pure oxygen. The OIT represents the time at the onset of the exhothermic oxidation process, whose rate can be inferred by referring to the time at the oxidation peak (see Fig. S2, Supplementary data). Each measurement was repeated at least three times on different portions of sample.

MALDI-TOF mass spectra were recorded in reflector mode using a Voyager-DE STR (Applied Biosystems) mass spectrometer equipped with a nitrogen laser emitting at 337 nm with a 3-ns pulse width and working in positive ion mode. The accelerating voltage was 20 kV; the grid voltage and the delay time were optimized for

each sample to achieve the higher molar mass values and the best resolution. The laser irradiance was maintained slightly above threshold. 2-(4-hydroxyphenilazo) benzoic acid (0.1 M in hexafluoroisopropanol (HFIP)) was used as matrix. Appropriate volumes of polymer solution (5 mg/ml in HFIP) and matrix solution were mixed to obtain 2:1, 1:1, and 1:2 ratios (sample/matrix v/v). 1 μL of each sample/matrix mixture was spotted on the MALDI sample holder and slowly dried to allow for matrix crystallization. Each measurement was repeated at least three times on different portions on sample.

3. Results

3.1. State of dispersion of the filler and impact on the thermal stability

Our first purpose was assessing the state of dispersion of the nanoparticles resulting from the melt compounding process. The shear and elongational stresses experienced by the material in the course of melt mixing promote the distribution and dispersion of the pristine clay aggregates inside the host polymer. In the borderline case in which the clay result perfectly dispersed in the form of its building blocks, i.e. individual silicate layers, the nanocomposite is referred as *exfoliated*. More often, stacks of several layers are still distinguishable at the end of the compounding step.

The internal structure of our sample PA11-C3 is shown in the TEM micrographs of Fig. 1. The clay is predominantly in the form of exfoliated lamellae; thin stacks made of few layers are also occasionally noticed.

The WAXD analyses shown in Fig. 2 confirm the absence of layered structures in the nanocomposite: the diffraction peak of the pristine clay at $2\theta \approx 4.8°$, corresponding to an inter-planar distance d_{001} of about 1.85 nm, disappears in the nanocomposite, the small

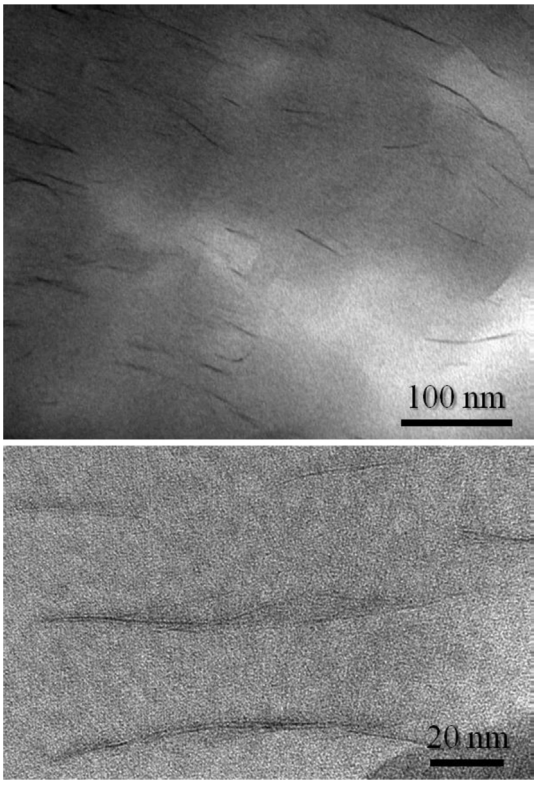

Fig. 1. Representative TEM micrographs of the sample PA11-C3.

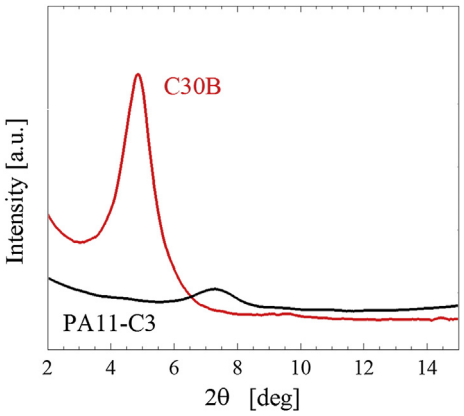

Fig. 2. WAXD patterns of Cloisite® 30B and the nanocomposite PA11 C3.

peak at $2\theta \approx 7.3°$ being the (001) refection of the α-form of PA11 [16].

The exfoliated morphology reflects in an improved thermal stability in both N_2 and air environment. This is shown in Table 1, where the results of TGA analyses are summarized.

Both the onset temperature of degradation and the temperature at the maximum derivative of weight loss increase by 15–20 °C with respect to the neat PA11. Such a result is typical of exfoliated nanocomposites, being usually ascribed to a barrier effect of the lamellae which hinders the diffusion of the volatile decomposition products [8]. In contrast, intercalated PA-clay nanocomposites usually exhibit comparable or even reduced thermal stability with respect to the unfilled matrix [17,18]. Consider now the high temperature residues. Taking into account a weight loss of ~27 wt.-% of pristine Cloisite® 30B due to the decomposition of the organomodifier [19], the values in Table 1 perfectly reflect the nominal composition.

After the state of dispersion of the nanoparticles has been detailed, we focus on the employ of rheology for studying the degradation of the polymer matrix in the melt state. Before starting our discussion, the effect of nanoparticles on the time evolution of the rheological properties of nanocomposites is briefly recalled in the next Section.

3.2. Effect of the nanoparticles on the time evolution of rheological properties

Extruded nanocomposite samples generally exhibit a certain degree of orientation of the plate-like clay particles. Further alignment is induced by the squeezing flow experienced during the preparation of the disks for the rheological analyses. This orientation is gradually lost when temperature is raised above the melting temperature of the matrix. The reason is that the lamellae are small enough to experience non-negligible Brownian motions,

Table 1
Onset temperature of degradation, temperature at maximum rate of decomposition and residual masses of PA11 and PA11-C3 as estimated through TGA analyses.

Sample	Gas	T_{95}[a] [°C]	T_{peak}[b] [°C]	Residue at T = 600 °C [wt.-%]
PA11	N2	390.7	438.8	1.1
PA11-C3		407.8	452.0	3.3
PA11	Air	395.2	441.5	1.0
PA11-C3		408.6	462.6	3.1

[a] Temperature at 5 wt.-% of weight loss.
[b] Temperature at the maximum derivative of weight loss.

progressively rearranging in the melt. As a result, the viscoelastic shear moduli increase over time due to many possible phenomena, namely nanoparticle rotation, flocculation and networking [20]. Whatever the dominant process, the timescale τ_f of such filler-induced change in the rheological properties is set by the rotary diffusivity of the lamellae, D_{r0}. Assuming the latter as rigid disks, we can roughly estimate τ_f as [21]:

$$\tau_f = D_{r0}^{-1} = \frac{4\eta_0 d^3}{3k_B T} \quad (1)$$

where η_0 is the zero-shear rate viscosity of the suspending medium, d is the disk diameter and k_B is the Boltzmann constant.

For a polymer melt like PA11, whose η_0 ranges between 10^2 and 10^3 Pa s at $T = 215$ °C, and assuming $d \sim 100 \div 300$ nm [22], one obtains $\tau_f \sim 10^2 \div 10^3$ s, that is comparable to the characteristic timescale for the degradation of the PA11 matrix [1]. In other words, in our samples filler- and polymer-induced alterations of the viscoelastic properties occur simultaneously, making challenging the interpretation of rheological data. Further complexity stems from the possible influence of the clay, and in particular of its organo-modifier, on the degradation kinetics of the host polymer. Aim of the next Sections is assessing the potential of viscoelastic analysis in discriminating between all these concomitant phenomena.

3.3. Time evolution of the rheological properties via TRMS

Our first objective is collecting reliable viscoelastic data as a function of time, so as to monitor the structural alterations occurring in the course of degradation. TRMS was used for this purpose. The time evolutions of the elastic moduli of the sample PA11-C3 in both N_2 and in air are shown in Fig. 3; the viscous moduli, less relevant to our purposes, are reported in the Supplementary data (Fig. S1).

Qualitative and quantitative differences emerge since the early stages of the tests. Let us first consider the sample treated in N_2 (Fig. 3a). G' noticeably grows during time, especially at low frequency and short times. The $G'(t)$ curve are smooth enough to allow for a reasonable estimate of the moduli at time-zero, i.e. before any phenomenon able to affect the rheological response has occurred. The extrapolation procedure described in *Part I* was used for this purpose. In brief, the $G'(t)$ and $G''(t)$ curves at the various frequencies are prolonged down to time zero by means of a straight line, whose slope is determined by interpolating the points collected at short times [1]. The extrapolated $G'(0)$ are shown in Fig. 3a as full red squares.

Consider now the sample treated in air (Fig. 3b). In this case, a peculiar two-steps growth of $G'(t)$ emerges at low frequency. Such a behavior may indicate the concurrence of different phenomena with distinct characteristic timescales. Another noteworthy aspect is the rapidity of the growth of $G'(t)$ in the early stages of the test. The initial slope of the curves in air is so steep to make difficult the estimate of $G'(0)$ by means of extrapolation. Rather, we use the same $G'(0)$ data of the sample treated in N_2. This is feasible because the $G'(0)$ data reflect the behavior of the "virgin" PA11-C3 sample and, as such, they prescind from the environment in which the tests are carried out. After the first rapid increase of G', a second process emerges after ~30 min, which causes a further, slower increase of elasticity.

The main differences between the samples treated in N_2 and in air concern the low frequencies. In this regime, the response of "slow" dynamic populations is probed. In case of pure polymers, the latter correspond to "large" structural units, at the limit, the entire polymer chain. In case of nanocomposites the filler itself exhibits an intrinsic elasticity, which adds up to that of the host polymer and emerges at low frequency, i.e. when the matrix is essentially relaxed. As a result, the time evolution of G' at low-frequency in nanocomposite samples contains information about both the polymer and nanoparticles. In our specific case, $G'(t)$ reflects (*i*) changes in the molecular architecture of PA11 due to degradation, and (*ii*) space rearrangements of the organo-clay, which moves in the host polymer melt towards more stable configurations. The issue that we are going to address is assessing the possibility of discriminating between these two contributions. To do so, the $G'(t)$ curves of PA11-C3 and neat PA11 are compared in Fig. 4 at the lowest and highest investigated frequency.

Let us begin our analysis by focusing on the high-frequency behavior. In this "fast" regime the presence of the filler simply causes an upward shift of G' without affecting its time dependence. This is essentially due to hydrodynamic interactions between the particles. Gleissle and Hochstein heuristically explained this mechanism by introducing the concept of *shear stress-equivalent inner shear rate*: the actual deformation experienced by the polymer confined in the small gap between contiguous particles is higher than what externally imposed, and the measured moduli are consequently higher than those of the unfilled polymer [23]. Since this effect only depends on the filler content, it is not surprising that negligible differences are found between the samples treated in N_2

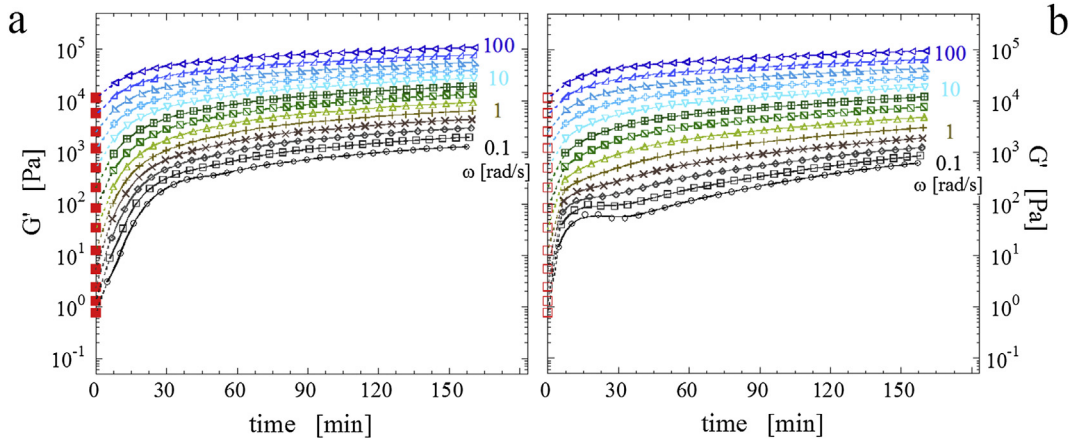

Fig. 3. Time evolution of the elastic moduli of PA11-C3 at $T = 215$ °C in N_2 (a) and in air (b). Red squares in (a) represent the extrapolated moduli at time-zero. The same data are shown as empty squares in (b). (For interpretation of the references to color in this figure legend, the reader is referred to the web version of this article.)

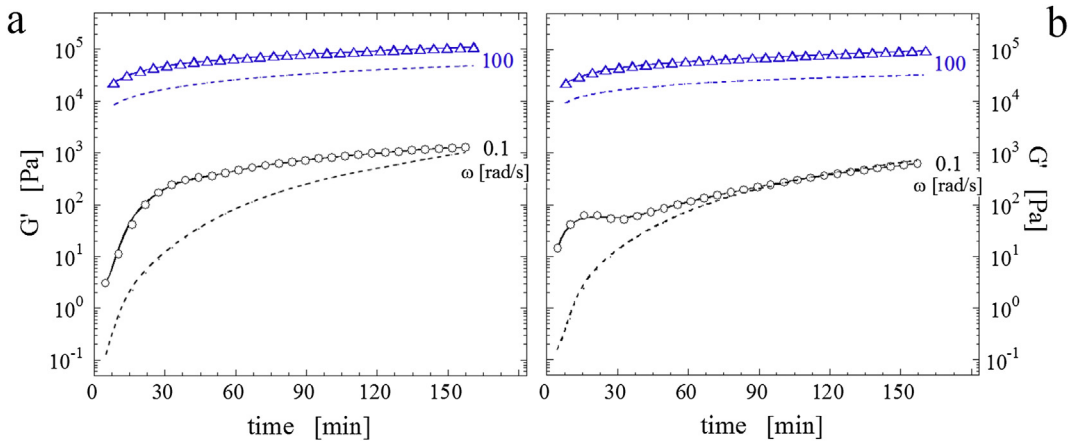

Fig. 4. Comparison between the $G'(t)$ curves in N_2 (a) and in air (b) of PA11-C3 (symbols) and neat PA11 (dashed lines) at $\omega = 0.1$ and 100 rad/s.

and in air.

The low-frequency modulus is much richer of information. As discussed before, over such longer timescales changes in the polymer architecture and space rearrangements of the nanoparticles are probed simultaneously. Isolating the two contributions to study them separately is difficult: they are not merely additional and can influence each other. More precisely, the nanoparticles can alter the degradation pathways of the matrix, and viscosity changes due to polymer degradation in turn affect the dynamics of the nanoparticles (see Equation (1)). Nonetheless, some important observations can be made based on the simple comparison between the $G'(t)$ curves of neat and clay-filled sample.

First of all, the amount of excess elasticity varies with time, i.e. the effect of the particles is not merely hydrodynamic. Clear differences emerge between the samples treated in N_2 and in air. In the former, the regularity of the $G'(t)$, systematically higher than that of the neat PA11, suggests a mere additional contribution of the nanoparticles. In contrast, the peculiar double-step growth of G' of PA11-C3 in air, as well as the crossing with the curve of neat PA11 at ~120 min, are clear signs of a direct effect of the nanoparticles on the degradation pathway of the polymer matrix. A further proof of this is the fast growth of G' in air in the very first moments of the test, i.e. when the nature of the gas surrounding the sample still has a negligible influence on the degradation kinetics. We can hence conclude that, besides rearranging in the host melt, the filler affects the degradation pathway of PA11 in air. Valuable information in this regard can be collected by looking at the frequency-dependent moduli discussed in the next Section.

3.4. Frequency response

The isochronal moduli in N_2 and air collected through the procedure described in *Part I* are shown in Fig. 5 at different instants. Note that the employ of TRMS ensures a high level of confidence on the viscoelastic curves.

Let us focus on the $G'(\omega)$ curves at low frequency, which are more relevant to our purposes. Initially, the growth of the elasticity in air is noticeably faster than in N_2: G' increases by ~2 orders of magnitude in only 5 min. In addition, the $G'(\omega)$ curves in air at short times exhibit a peculiar upwards concavity. The latter disappears after ~30 min, i.e. when a second process emerges as a distinct shoulder in the low-frequency $G'(t)$ curves in air (see Fig. 3b). From that point on, the moduli in N_2 result systematically higher than those in air.

Consider now the isochronal complex viscosity curves, which are shown in Fig. 6 at different instants. Valuable information about the molecular architecture of neat PA11 was collected in *Part I* by fitting a simple Carreau-like equation with a yield stress to the $\eta^*(\omega)$ data [1]. In brief, the zero-frequency complex viscosity η_0^* was correlated to the mass average molecular weight M_w, while an upturn of η^* at low frequency was identified as the rheological fingerprint of insoluble fractions of cross-linked polymer. The latter was correlated to the value of yield stress σ_0 required to fit the experimental η^* curves.

Here we abstain from modeling the $\eta^*(\omega)$ data of the nanocomposite sample PA11-C3, whose relaxation spectrum is considerably more complex than that of neat polymers. Nonetheless, useful insights into the degradation mechanisms can be obtained by means of an accurate comparison of the rheological curves in N_2 and in air.

Let us focus on the behavior in the early stages of the test. An upturn of η^* is identified after 5, 10 and 15 min in air. In principle, nanoparticle networks can impart a yield stress to the nanocomposite. However, we can exclude this occurrence because the $\eta^*(\omega)$ curves in N_2 do not exhibit any upturn. Rather, we explain this effect as the result of premature cross-linking induced by the nanoparticles. Oxygen is essential to this process, which is not observed in N_2. This means that this nanoparticle-induced cross-linking mainly concerns the outer shell of the sample, i.e. the surface in direct contact with air. A similar conclusion was drawn for neat PA11, but in that case appreciable yield stresses were only noticed after ~60 min in air [1]. Okamba-Diogo et al. proposed that cross-linking of neat PA11 begins after an induction time since reactions among primary oxidation products are involved [24]. In the case of PA11-C3, we can speculate that nanoparticles somehow accelerate such preliminary steps for cross-linking, which hence appears in the rheological curves since the early stages of the tests. As will be discussed in Section 3.4, the chemical mechanism involves radical species deriving from the thermo-oxidative degradation of the clay organo-modifier [25]. It is interesting to notice that the upturn of η^* progressively diminishes, eventually disappearing in about 30 min. In contrast, we found that, once activated, cross-linking in neat PA11 proceeds quite rapidly [1]. The reason is that a distinct process, namely the space rearrangements of the organo-clay, overlaps and eventually shields the effect of polymer cross-linking. This issue will be specifically addressed in Section 3.5. Before, the picture emerged from rheological analysis is corroborated through targeted analytical techniques in the next Section.

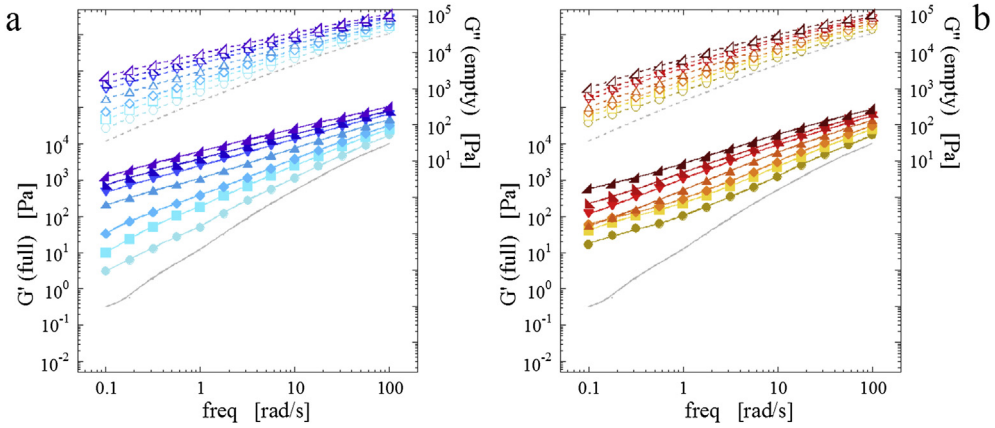

Fig. 5. Isochronal elastic (full symbols, left axis) and viscous (empty symbols, right axis) moduli of PA11-C3 treated in N_2 (a) and in air (b) at different instants: 5 (circles), 10 (squares), 15 (diamonds), 30 (triangles), 60 (reverse triangles), 90 (half-square left), and 150 (half-square right) min. Gray lines are the elastic (continuous) and viscous (dashed) moduli extrapolated at time-zero.

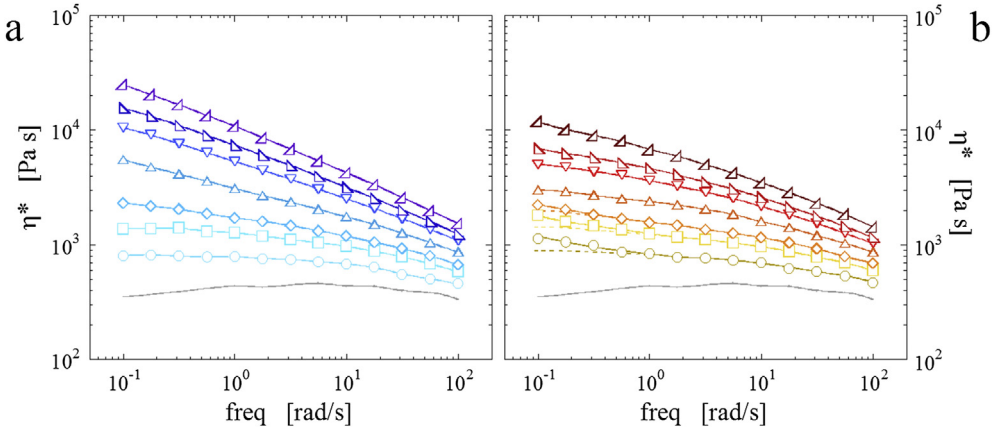

Fig. 6. Isochronal complex viscosity of PA11-C3 treated in N_2 (a) and in air (b) at different instants: 5 (circles), 10 (squares), 15 (diamonds), 30 (triangles), 60 (reverse triangles), 90 (half-square left), and 150 (half-square right) min. Dashed lines in (b) highlight the upturn of η^* at low frequency; continuous lines in (a) and (b) are the complex viscosities at time-zero.

3.5. Degradation kinetics and reaction mechanisms through OIT and MALDI-TOF analyses

The comparison with the rheological behavior of the neat PA11 enabled us to draw some conclusions about the degradation of the polymer matrix in the nanocomposite sample PA11-C3. To sum up, rheological data suggest that the nanoparticles boost up thermo-oxidation, promoting early cross-linking on the surface of the sample treated in air. In contrast, little can be said about the nanocomposite sample treated in N_2. In this case, the excess of elasticity could simply reflect the additional contribution of the nanoparticles.

Targeted analyses were performed to verify the correctness of the previous hypotheses and to shed light on the degradation pathways. Consider the sample treated in air. The results of OIT measurements are summarized in Table 2, where the behavior of the nanocomposite is compared to that of the neat polymer (see also Supplementary data, Fig. S2). In both samples thermo-oxidation begins in a few seconds. The nanoparticles slightly delay the OIT, probably because of a barrier effect to oxygen diffusion. Nevertheless, the comparison of the times at the oxidation peak (t_2) reveals that, once started, thermo-oxidation is much faster in the nanocomposite.

Table 2
Onset of the thermo-oxidation process (t_1) and time at the oxidation peak (t_2). The interval t_2-t_1 gives a measure of the rate of the thermo-oxidation process.

Sample	t_1 (OIT) [s]	t_2 [s]
PA11	16.6 ± 0.2	166 ± 14
PA11-C3	23.8 ± 3.3	78 ± 3

Once confirmed that thermo-oxidation is actually faster in the presence of nanoparticles, we focus our attention on the nature of the thermo-oxidative reactions. MALDI-TOF analyses were performed on samples dissolved in HFIP after having been treated in air for different time. The amount of insoluble gel, not analyzable by MALDI, was quantified as well. A detailed discussion of the MALDI spectra is beyond the purposes of the present study. Here we simply observe that a correlation can be established between the amount of insoluble gel and the appearance in the MALDI spectra of a peak assigned to $NH_2/CONH_2$ oligomers (mass to charge ratio $m/z = 1322.1519$). The intensity of such signal is shown in Fig. 7 as a function of time, together with the estimated amount of insoluble gel.

In both samples the peak intensity initially grows with time, and then the signal decreases until vanishing. Appreciable amounts of

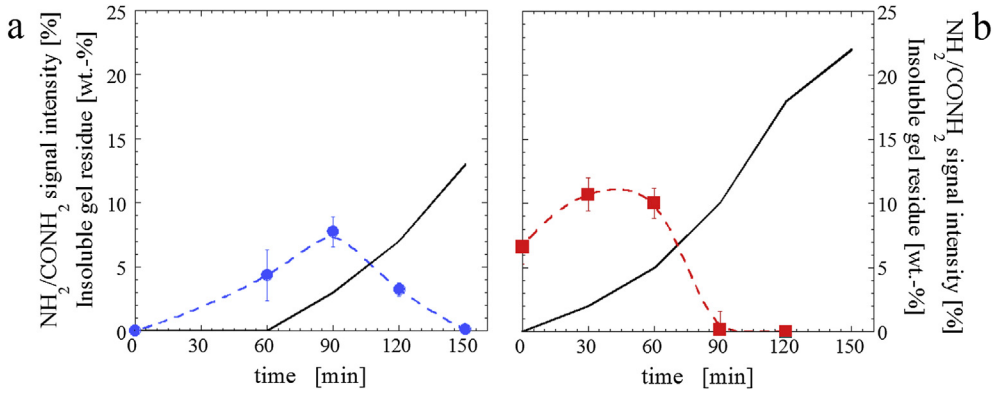

Fig. 7. Intensity of the MALDI peak assigned to $NH_2/CONH_2$ oligomers as a function of time for the samples PA11 (a) and PA11-C3 (b) treated in air; dashed lines are guides for the eye. The amount of insoluble gel is shown as continuous lines.

insoluble gel become detectable when the MALDI peak is approximately at its maximum. This suggests that $NH_2/CONH_2$ species are directly involved in the cross-linking reactions, being progressively consumed as the insoluble gel forms. The well-known reaction schemes for cross-linking of polyamide, here readapted for PA11, are reported as Supplementary data (see Fig. S3). The comparison between neat PA11 and PA11-C3 reveals that cross-linking is much faster in the presence of nanoparticles. In particular, signals of $NH_2/CONH_2$ oligomers were clearly detected even in the as-extruded PA11-C3 sample, i.e. at time zero. The enhanced cross-linking in the presence of nanoparticles is a consequence of the thermo-oxidative degradation of the organo-modifier of Cloisite® 30B. In detail, Hofmann elimination reaction of bis(2-hydroxylethyl) methyl tallow alkylammonium produce α-olefins, which in turn react in air producing oxygenated species (aldehydes, acids) as final products. In the initial step of auto-oxidation, the formation of α-olefin hydroperoxides entails the capture of available hydrogen atoms. The most favorable site for the attack is the α-amino methylene position of PA11 chains. At this point, the well-known α-CH hydrogen abstraction mechanism proceeds, thus accelerating cross-linking. We can also speculate a possible contribution of aldehydes produced by oxidation of α-olefins according to the Karsten and Rossback mechanism [26]. In this case the formation of unsaturated oligoenimine structures is also promoted.

Besides cross-linking, nanoparticle-induced thermo-oxidation brings about chain scission phenomena, which reflect in the MALDI spectra as persistent signals assigned to $NH_2/COOH$ linear oligomers. The reduction in molecular weight has a detrimental effect on the elasticity of the nanocomposite, whose low-frequency G' becomes lower than that of the neat matrix over long times ($t >$ 120 min) (see Fig. 4b).

Finally, let us consider the nanocomposite treated in N_2. Neither insoluble gel residue nor specific MALDI peaks were detected in this case. As in pure PA11, non-oxidative thermal degradation of the nanocomposite mainly entails post-condensation reactions. The rheological effect of the growth in the molecular weight is an in-crease of G' at low frequency, which results simply higher than that of pure PA11 because of the additional elastic contribution of the nanoparticles (see Fig. 4a).

3.6. *Effect of nanoparticle content*

The previous section demonstrates that rheology provides valuable information about polymer degradation even in case of materials such as nanocomposites, whose rheological response is substantially modified by the nanoparticles. Aim of this section is investigating the limits of rheological analysis in case of superimposed contributions.

As discussed in Section 3.3, the rheological fingerprint of polymer cross-linking in the sample treated in air, namely the upturn of the $\eta^*(\omega)$ curves at low frequency, disappears in ~30 min. On the other hand, we found that the amount of cross-linked polymer keeps increasing up to 150 min (see Fig. 7). This apparent inconsistency can be explained by invoking the superposition of the rheological contributions due to space rearrangement of the nanoparticles and cross-linking. Specifically, we argue that the overall rheological response can be roughly considered as the sum of the independent contributions of polymer degradation and nanoparticle mobility, being dominated by the more intense of the two phenomena. If this simplified picture holds, then increasing the nanoparticle loading should eventually mask the effect of polymer degradation. To verify this idea, the rheological behavior of the nanocomposite samples containing 9 wt.-% of organo-clay was investigated. A comparison between selected $G'(t)$ and $\eta^*(\omega)$ curves in N_2 and in air is shown in Fig. 8. The complete families of curves are reported as Supplementary data (Fig. S4–S6).

In the first 60 min the curves in N_2 and in air are indistinguishable, meaning that the rheological response in the highly filled PA11-C9 sample is dominated by the particles. This means that rheology does not provide information about polymer degradation for such high filler loadings, at least in the first hour of treatment. Differences only emerge over longer times, i.e. when more radical alterations occur in the rheology of the polymer matrices. In particular, the moduli in N_2 keep increasing as a result of the progress of post-condensation reactions. The growth is less pronounced in air because of concomitant chain scission phenomena, which were found to have detrimental effect over long times even in the sample PA11-C3.

4. Conclusions

TRMS has been employed for monitoring the progress of thermal and thermo-oxidative degradation of PA11 in a sample containing organo-clay (Cloisite® 30B) as filler. TEM and WAXD analyses prove that the nanocomposite exhibits predominantly exfoliated morphology. On the one hand, the good dispersion of the nanoparticles brings about a significant improvement of thermal stability at high temperature, which has been estimated through TGA analyses. On the other hand, the exfoliated nanoparticles remarkably alter the rheology of the nanocomposite, making it difficult to isolate the contribution due to the degradation of the polymer matrix. Nonetheless, a careful rheological analysis

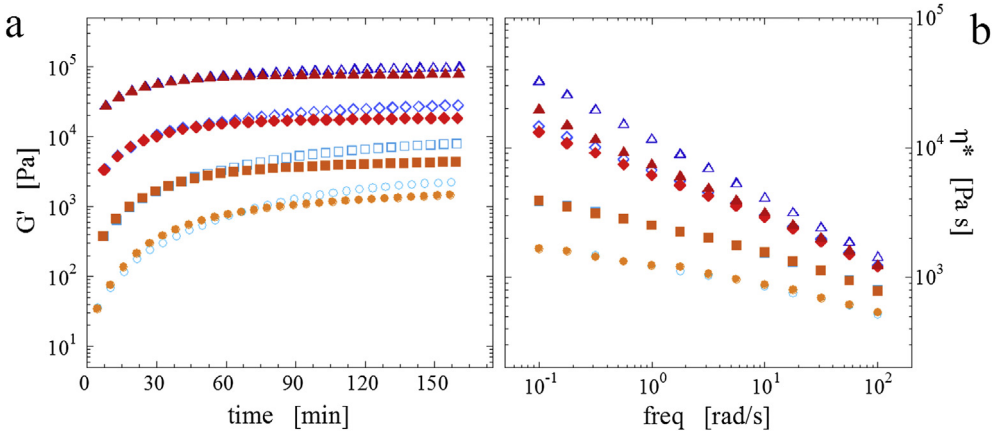

Fig. 8. (a) Time evolution of the elastic moduli of PA11-C9 at $T = 215$ °C in N_2 (empty symbols) and in air (full symbols) at selected frequencies: 0.1 (circles), 1 (squares), 10 (diamonds), and 100 (traingles) rad/s. (b) Isochronal complex viscosity of PA11-C9 treated in N_2 (empty symbols) and in air (full symbols) at different instants: 5 (circles), 15 (squares), 60 (diamonds), and 150 (triangles) min.

grounded on TRMS enabled us to infer information about PA11 degradation despite the additional contribution of the nanoparticles. Essentially the same degradation mechanisms as in neat PA11 have been identified for the nanocomposite, namely post-condensation (in N_2), hydrolysis and cross-linking (in air) reactions. However, nanoparticles accelerate PA11 thermo-oxidative degradation. In particular, the rheological fingerprint of PA11 cross-linking, namely a yield stress in the complex viscosity curve, was noticed since the early stages of treatment in air in the presence of nanoparticles. OIT measurements have confirmed the hypotheses based on rheological analysis. In addition, MALDI-TOF investigations have clarified the chemical aspects of PA11thermo-oxidation, highlighting the key-role played by the clay organo-modifier. Overall, rheology confirms to be a precious tool for studying polymer degradation even in case of rheologically complex systems such as polymer nanocomposites. However, investigations carried out on a system at higher filler loading have revealed that valuable information about polymer degradation can be actually gathered only provided that the filler disturbance is not so high to mask the rheological response of the polymer matrix.

Acknowledgments

This work was supported by the FIRB 2010—Futuro in ricerca project (No. RBFR10DCS7) funded by the Italian Ministry of University and Research (MIUR).

Appendix A. Supplementary data

Supplementary data related to this article can be found on line.

References

[1] G. Filippone, S.C. Carroccio, R. Mendichi, L. Gioiella, N. TZ Dintcheva, C. Gambarotti, Time-resolved rheology for studying polymer degradation in the melt state – part I: thermal and thermo-oxidative degradation of polyamide 11, Polymer 72 (2015) 134–141, http://dx.doi.org/10.1016/j.polymer.2015.06.059.
[2] S. Srivastava, J.L. Schaefer, Z. Yang, Z. Tu, L.A. Archer, 25th anniversary article: polymer–particle composites: phase stability and applications in electrochemical energy storage, Adv. Mater. 26 (2) (2014) 201–234, http://dx.doi.org/10.1002/adma.201303070.
[3] M.A. Treece, J.P. Oberhauser, Soft glassy dynamics in polypropylene-clay nanocomposites, Macromolecules 40 (3) (2007) 571–582, http://dx.doi.org/10.1021/ma0612374.
[4] X. Wang, P. Sun, G. Xue, H.H. Winter, Late-state ripening dynamics of a polymer/clay nanocomposite, Macromolecules 43 (4) (2010) 1901–1906, http://dx.doi.org/10.1021/ma901665m.
[5] P. Cassagnau, Linear viscoelasticity and dynamics of suspensions and molten polymers filled with nanoparticles of different aspect ratios, Polymer 54 (18) (2013) 4762–4775, http://dx.doi.org/10.1016/j.polymer.2013.06.012.
[6] A.P. Kumar, D. Depan, N.S. Tomer, R.P. Singh, Nanoscale particles for polymer degradation and stabilization—trends and future perspectives, Prog. Polym. Sci. 34 (6) (2009) 479–515, http://dx.doi.org/10.1016/j.progpolymsci.2009.01.002.
[7] J.K. Pandey, K.R. Reddy, A.P. Kumar, R.P. Singh, An overview on the degradability of polymer nanocomposites, Polym. Degrad. Stab. 88 (2) (2005) 234–250, http://dx.doi.org/10.1016/j.polymdegradstab.2004.09.013.
[8] M. Alexandre, P. Dubois, Polymer-layered silicate nanocomposites: preparation, properties and uses of a new class of materials, Mater. Sci. Eng. R Rep. 28 (1) (2000) 1–63, http://dx.doi.org/10.1016/S0927-796X(00)00012-7.
[9] R. Krishnamoorti, K. Yurekli, Rheology of polymer layered silicate nanocomposites, Curr. Opin. Colloid Interface Sci. 6 (5–6) (2001) 464–470, http://dx.doi.org/10.1016/S1359-0294(01)00121-2.
[10] P. Cassagnau, Melt rheology of organoclay and fumed silica nanocomposites, Polymer 49 (9) (2008) 2183–2196, http://dx.doi.org/10.1016/j.polymer.2007.12.035.
[11] T.D. Fornes, P.J. Yoon, D.R. Paul, Polymer matrix degradation and color formation in melt processed nylon 6/clay nanocomposites, Polymer 44 (24) (2003) 7545–7556, http://dx.doi.org/10.1016/j.polymer.2003.09.034.
[12] K. Stoeffler, P.G. Lafleur, J. Denault, Thermal decomposition of various alkyl onium organoclays: effect on polyethylene terephthalate nanocomposites' properties, Polym. Degrad. Stab. 93 (7) (2008) 1332–1350, http://dx.doi.org/10.1016/j.polymdegradstab.2008.03.029.
[13] X. Xu, Y. Ding, Z. Qian, F. Wang, B. Wen, H. Zhou, S. Zhang, M. Yang, Degradation of poly (ethylene terephthalate)/clay nanocomposites during melt extrusion: effect of clay catalysis and chain extension, Polym. Degrad. Stab. 94 (1) (2009) 113–123, http://dx.doi.org/10.1016/j.polymdegradstab.2008.09.009.
[14] N. Najafi, M.C. Heuzey, P.J. Carreau, P.M. Wood-Adams, Control of thermal degradation of polylactide (PLA)-clay nanocomposites using chain extenders, Polym. Degrad. Stab. 97 (4) (2012) 554–565, http://dx.doi.org/10.1016/j.polymdegradstab.2012.01.016.
[15] S. Carroccio, C. Puglisi, G. Scaltro, T. Ferreri, G. Montaudo, Matrix-assisted laser desorption/ionization time-of-flight investigation of Nylon 6 and Nylon 66 thermo-oxidation products, Eur. J. Mass Spectrom. 13 (6) (2008) 397–408, http://dx.doi.org/10.1255/ejms.899.
[16] Q. Zhang, Z. Mo, H. Zhang, S. Liu, S.Z. Cheng, Crystal transitions of Nylon 11 under drawing and annealing, Polymer 42 (13) (2001) 5543–5547, http://dx.doi.org/10.1016/S0032-3861(01)00050-7.
[17] T. Liu, K.P. Lim, W.C. Tjiu, K.P. Pramoda, Z.K. Chen, Preparation and characterization of nylon 11/organoclay nanocomposites, Polymer 44 (12) (2003) 3529–3535, http://dx.doi.org/10.1016/S0032-3861(03)00252-0.
[18] K.P. Pramoda, T. Liu, Z. Liu, C. He, H.J. Sue, Thermal degradation behavior of polyamide 6/clay nanocomposites, Polym. Degrad. Stab. 81 (1) (2003) 47–56, http://dx.doi.org/10.1016/S0141-3910(03)00061-2.
[19] J.M. Cervantes-Uc, J.V. Cauich-Rodríguez, H. Vázquez-Torres, L.F. Garfias-Mesías, D.R. Paul, Thermal degradation of commercially available organoclays studied by TGA–FTIR, Thermochim. Acta 457 (1) (2007) 92–102, http://dx.doi.org/10.1016/j.tca.2007.03.008.
[20] G. Filippone, A. Causa, M.S. de Luna, L. Sanguigno, D. Acierno, Assembly of plate-like nanoparticles in immiscible polymer blends–effect of the presence of a preferred liquid–liquid interface, Soft Matter 10 (18) (2014) 3183–3191, http://dx.doi.org/10.1039/C3SM52995A.
[21] R.G. Larson, The Structure and Rheology of Complex Fluids. Chapter 6:

Particulate Suspensions, Oxford University Press, 1999, pp. 263–323.
[22] H.J. Ploehn, C. Liu, Quantitative analysis of montmorillonite platelet size by atomic force microscopy, Ind. Eng. Chem. Res. 45 (21) (2006) 7025–7034, http://dx.doi.org/10.1021/ie051392r.
[23] W. Gleissle, B. Hochstein, Validity of the Cox–Merz rule for concentrated suspensions, J. Rheol. (1978-present) 47 (4) (2003) 897–910, http://dx.doi.org/10.1122/1.1574020.
[24] O. Okamba-Diogo, E. Richaud, J. Verdu, F. Fernagut, J. Guilment, B. Fayolle, Molecular and macromolecular structure changes in polyamide 11 during thermal oxidation, Polym. Degrad. Stab. 108 (2014) 123–132, http://dx.doi.org/10.1016/j.polymdegradstab.2014.05.028.
[25] W. Xie, Z. Gao, W.P. Pan, D. Hunter, A. Singh, R. Vaia, Thermal degradation chemistry of alkyl quaternary ammonium montmorillonite, Chem. Mater. 13 (9) (2001) 2979–2990, http://dx.doi.org/10.1021/cm010305s.
[26] T. Karstens, V. Rossbach, Thermo-oxidative degradation of polyamide 6 and 6, 6. Structure of UV/VIS-active chromophores, Die Makromol. Chem. 191 (4) (1990) 757–771, http://dx.doi.org/10.1002/macp.1990.021910404.